J Intell Robot Syst (2013) 69:417–429
DOI 10.1007/s10846-012-9737-y

Ground Target Tracking Using UAV with Input Constraints

Senqiang Zhu · Danwei Wang · Chang Boon Low

Received: 1 July 2012 / Accepted: 13 July 2012 / Published online: 4 August 2012

Abstract This paper provides a solution to the problem of ground target tracking using an unmanned aerial vehicle (UAV) with control input constraints. Target tracking control with input constraints is an important and challenging topic in the study of UAVs. In order to achieve precise target tracking in the presence of constant background wind and target motion, this paper proposes a saturated heading rate controller based on a guidance vector field while the airspeed is held constant. This proposed approach guarantees the global convergence of the UAV to a desired circular orbit around a target. To estimate unknown constant background wind and target motion, an adaptive observer with bounded estimate is developed. Simulation results demonstrate the effectiveness of the proposed approach.

S. Zhu · D. Wang (✉)
Faculty of School of EEE,
Nanyang Technological University,
Singapore 639798, Singapore
e-mail: edwwang@ntu.edu.sg

S. Zhu
e-mail: zhus0009@ntu.edu.sg

C. Boon Low
DSO National Laboratories, INFO Division,
Manned-Unmanned Programme, 27 Medical Drive,
Singapore 117510, Singapore
e-mail: lchangbo@dso.org.sg

Keywords Target tracking · UAV · Input constraints · Adaptive estimation

1 Introduction

In recent years, the research of UAVs has received much attention, as there are many potential applications in both military and civilian fields [2, 4, 6, 7]. Ground target tracking is an important application of UAVs, and several control strategies have been developed in the literature, such as vector field approach [9, 11], good helmsman approach [18], MPC based approach [3], etc. Despite great progress has been made, practical and theoretical challenges are still abundant. Therefore, this paper will focus on the problem of ground target tracking using a fixed wing UAV with control input constraints.

In [12] and [13], Park et al. propose a nonlinear guidance logic to achieve path following for curved trajectory. In this approach, a reference point on the desired path is designated, and a lateral acceleration command is generated according to the direction of the reference point with respect to the vehicle velocity. In [10], target tracking using a mobile robot is proposed, where global asymptotical stability is guaranteed. In [18], "good helmsman" approach is introduced to achieve path following. In this approach, the vehicle kinematics is represented by a Serret-

Frenet formulation in terms of path parameters, and then a course rate controller is designed to bring the UAV from its current path to the desired path in the Serret-Frenet frame. Furthermore, in order to estimate the unknown wind, a linear observer is constructed. However, the estimate of the unknown wind is not bounded. Rafi et al. [15] propose an autonomous navigation algorithm to guide the UAV with physical constraints to follow a moving target.

Recently, Lyapunov guidance vector field approaches, which stem from potential field work, are introduced to guide the UAV to achieve target tracking [5, 8, 9, 11, 20]. In [11], the desired course angle of the UAV is generated by using a Lyapunov vector field approach. A sliding mode course rate controller is applied to track the desired course angle so that the UAV achieves circular target tracking. In [8], a heading rate controller is used to track the desired heading generated by a vector field approach while holding a constant airspeed. However, the control input constraints are not explicitly considered in the proof. Another different Lyapunov guidance vector field approach is introduced in [5] to guide the UAV to fly a circular orbit around a target. Both stationary target tracking and moving target tracking are studied based on the proposed Lyapunov guidance vector field. Based on the work in [5], Summers et al. [20] provide the formal proof of heading and standoff radius convergence with heading error located in the second and third quadrants. Moreover, they propose an adaptive approach to estimate the unknown background wind and target motion. However, the proof for the global convergence of the UAV to the desired orbit is still lack. The recent study in [21] proposes an adaptive control approach to achieve standoff target tracking in the presence of unknown background wind and target motion. In this approach, a variable heading rate controller is utilized while the airspeed is held constant. However, the heading rate input constraint is not taken into account.

This paper studies the problem of ground target tracking using a fixed wing UAV with control input constraints. The motion of the fixed wing UAV with lower level autopilots (altitude hold, velocity hold and heading rate hold autopilots) is described by its kinematic model. Background wind and target motion are considered during controller design. A guidance vector field is introduced to generate the desired relative course angle. Based on this vector field, a saturated heading rate controller, accounting for the physical constraint of the UAV, is proposed to regulate the actual relative course angle to the desired one while the airspeed is held constant. This proposed approach guarantees that the UAV with an arbitrary initial state can asymptotically converge to a desired circular orbit around the target. A rigorous proof for global convergence is also provided in this paper. In order to estimate unknown constant background wind and target motion, an adaptive observer is developed to guarantee bounded estimate.

The remainder of this paper is organized as follows. Section 2 introduces the UAV model and the guidance vector field approach. Section 3 proposes a saturated heading rate controller, and the complete proof for the convergence of the UAV to the desired circular orbit is provided. In Section 4, an adaptive observer for unknown wind and target motion is developed. In Section 5, the proposed approach is illustrated via the simulation results. Finally, the conclusions are given in Section 6.

2 Problem Statement

In this section, a commonly used UAV model [1, 14] with control input constraints is firstly introduced. Then the desired relative course rate is derived based on a guidance vector field. After that, the condition that the desired relative course rate reaches saturation will be analyzed.

2.1 UAV Model

This paper assumes that the altitude of the UAV is held constant. The kinematic model describing the relative motion of an UAV with respect to a moving target in the presence of background wind is given by the following equations

$$\begin{aligned} \dot{x}_r &= u_1 \cos\psi + W_x - \dot{x}_t \\ \dot{y}_r &= u_1 \sin\psi + W_y - \dot{y}_t \\ \dot{\psi} &= u_2 \end{aligned} \tag{1}$$

where, as illustrated in Fig. 1, $(x_r, y_r) \in \mathbb{R}^2$ is the two-dimensional relative position of the fixed wing UAV with respect to the moving target, $\psi \in [-\pi, \pi)$ is the UAV heading angle, $(\dot{x}_t, \dot{y}_t) \in \mathbf{R}^2$ is target velocity, $(W_x, W_y) \in \mathbf{R}^2$ is background wind velocity and u_1, u_2 are the two control input signals which are commanded airspeed and heading rate respectively.

Due to the stall condition, the thrust limitation and the roll angle limitation of the fixed wing UAV [16, 17], the following input constraints should be enforced on the UAV

$$0 < v_{\min} \le u_1 \le v_{\max}; \ |u_2| \le \omega_{\max}. \tag{2}$$

Note from the UAV model 1 that, target velocity and background wind velocity affect the UAV kinematics in the same way. For the sake of simplicity, these two velocities can be combined to a single velocity term $(T_x, T_y) = (\dot{x}_t - W_x, \dot{y}_t - W_y)$ which is called moving target velocity [5] in the following content. The kinematic model of the UAV can be rewritten as

$$\begin{aligned} \dot{x}_r &= u_1 \cos\psi - T_x, \\ \dot{y}_r &= u_1 \sin\psi - T_y, \\ \dot{\psi} &= u_2. \end{aligned} \tag{3}$$

In this paper, it is assumed that the airspeed is held constant, i.e. $u_1 = v_0$, as well as that the moving target velocity is constant and slower than the airspeed, i.e. $T_x^2 + T_y^2 < v_0^2$. By combining the moving target velocity with the airspeed, the following UAV kinematic model is obtained:

$$\dot{x}_r = v_r \cos\chi, \ \dot{y}_r = v_r \sin\chi, \ \dot{\chi} = \lambda(\psi) u_2 \tag{4}$$

where χ denotes the relative course angle depicted in Fig. 1, v_r denotes the relative speed, and

$$v_r = \left(v_0^2 + T_x^2 + T_y^2 - 2v_0(T_x \cos\psi + T_y \sin\psi)\right)^{\frac{1}{2}},$$

$$\chi = \arctan 2(v_0 \sin\psi - T_y, v_0 \cos\psi - T_x),$$

$$\lambda(\psi) = \frac{v_0^2 - v_0(T_x \cos\psi + T_y \sin\psi)}{v_r^2} \ge \frac{1}{2}.$$

The UAV model can also be expressed in polar coordinates as

$$\begin{aligned} \begin{bmatrix} \dot{r} \\ r\dot{\theta} \end{bmatrix} &= \begin{bmatrix} \dot{x}_r \cos\theta + \dot{y}_r \sin\theta \\ -\dot{x}_r \sin\theta + \dot{y}_r \cos\theta \end{bmatrix} \\ &= \begin{bmatrix} v_r \cos(\chi - \theta) \\ v_r \sin(\chi - \theta) \end{bmatrix} \end{aligned} \tag{5}$$

where $r = (x_r^2 + y_r^2)^{\frac{1}{2}}$ is the horizontal distance between the UAV and the target, and θ is the clock angle (see Fig. 1).

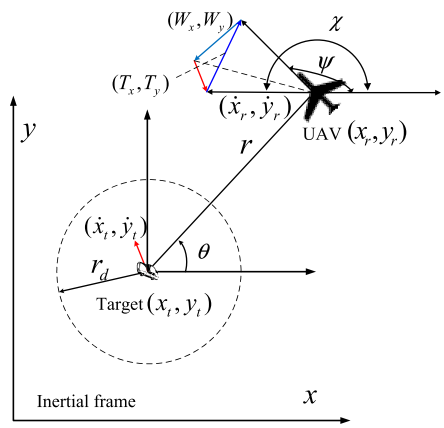

Fig. 1 Geometry of ground target tracking in wind

2.2 Guidance Vector Field

Guidance vector field is utilized to generate a desired relative course angle which guides the UAV to fly around a designated ground target with a desired distance r_d. A guidance vector field which is similar to that in [5] is introduced as follows:

$$\chi_d = \theta + \phi \tag{6}$$

where $\theta = \begin{cases} \arctan2(y_r, x_r) & \text{if} \quad r > 0 \\ \chi & \text{if} \quad r = 0 \end{cases}$ and $\phi = 2\arctan(\frac{r}{r_d})$.

From Eq. 6, it can be observed that when $r \to 0$, the desired relative course angle approaches the direction along the radius away from the origin, and when $r \to \infty$, the desired relative course directly points to the origin. It can also be known that the desired relative course angle is discontinuous at the point $r = 0$. It will be shown that if the UAV follows this vector field, then it will converge to the desired circular orbit asymptotically. Consider the following Lyapunov function candidate

$$V(r) = (r - r_d)^2. \tag{7}$$

Differentiating this Lyapunov function leads to the following equation

$$\dot{V} = 2(r - r_d)\dot{r} = -\frac{2v_r(r - r_d)^2(r + r_d)}{r^2 + r_d^2} \leq 0. \quad (8)$$

By LaSalle invariance principle, r asymptotically converges to the desired distance r_d. It is worth noting that the above result is derived under the assumption that the relative course angle is aligned with the desired relative course angle generated by the vector field. However, there generally exists an angle error between the actual relative course angle and the desired relative course angle. The relative course error can be defined by

$$\chi_e = \chi - \chi_d \in [-\pi, \pi). \quad (9)$$

When $r > 0$, the desired relative course rate can be obtained by taking the derivative of Eq. 6 as

$$\begin{aligned}\dot{\chi}_d &= \dot{\theta} + \dot{\phi} = \frac{v_r}{r}\sin(\chi - \theta) + \frac{\partial \phi}{\partial r}\dot{r} \\ &= \frac{v_r}{r}[\sin(\chi_e + \phi) + \sin(\phi)\cos(\chi_e + \phi)]. \end{aligned} \quad (10)$$

It is observed from Eq. 10 that when $r \to 0$, $\dot{\chi}_d$ may approach infinity while there exists a relative course error. When $r = 0$, the desired relative course rate can not be derived from Eq. 6. Thus, this paper defines the desired relative course rate at the point $r = 0$ as follows:

$$\dot{\chi}_d = \frac{4v_r}{r_d}. \quad (11)$$

In order to guarantee that the desired relative course rate without relative course error is feasible to track, it is assumed that the maximum heading rate satisfies the following condition:

$$w_{\max} \geq \frac{4(v_0 + (T_x^2 + T_y^2)^{\frac{1}{2}})^2}{v_0 r_d}. \quad (12)$$

3 Ground Target Tracking

This section focuses on designing the heading rate controller to achieve ground target tracking. A saturated heading rate controller is proposed and the global convergence of target tracking is rigorously proved.

Due to the physical constraint of the fixed wing UAV, the heading rate control input may reach saturation. In this paper, a new saturated heading rate controller is proposed as follows:

$$u_2 = \begin{cases} w & \text{if } |w| \leq w_{\max} \\ sgn(w)w_{\max} & \text{if } |w| > w_{\max} \end{cases} \quad (13)$$

where $w = -k\chi_e + \frac{\dot{\chi}_d}{\lambda(\psi)}$ and $k > 0$. Formula 13 shows that, the proposed controller includes a feedback term and a feedforward term when it is not saturated. Obviously, this controller satisfies the kinematic constraint of the fix wing UAV.

In this paper, the airspeed of the UAV is assumed to be constant. However, the relative speed v_r varies as the heading changes. Moreover, the variation of the relative speed has a significant influence on the relative course rate. Therefore, the relation between the relative speed and the heading has to be explored. The following lemma is introduced to indicate this relation.

Lemma 1 *If the moving target velocity is slower than the airspeed, i.e.,* $v_0^2 \geq T_x^2 + T_y^2$ *, then* $\frac{v_r}{\lambda(\psi)} \leq \frac{(v_0 + (T_x^2 + T_y^2)^{\frac{1}{2}})^2}{v_0}$.

Proof By assumption, the moving target velocity and the airspeed of the UAV are constant. Thus, ψ is the only variable in v_r and $\lambda(\psi)$. Let

$$\begin{aligned} f(\psi) &= \frac{v_r}{\lambda(\psi)} \\ &= \frac{(v_0^2 + T_x^2 + T_y^2 - 2v_0(T_x\cos\psi + T_y\sin\psi))^{\frac{3}{2}}}{v_0^2 - v_0(T_x\cos\psi + T_y\sin\psi)} \end{aligned}$$

For the sake of simplicity, the following notations are introduced: $T = (T_x^2 + T_y^2)^{\frac{1}{2}}$, $\eta = \arctan2(T_x, T_y)$ and $\xi = \sin(\psi + \eta)$. Then $f(\psi)$ can be rewritten as

$$f(\psi) = \frac{(v_0^2 + T^2 - 2v_0 T\xi)^{\frac{3}{2}}}{v_0^2 - v_0 T\xi} \quad (14)$$

Differentiating the function $f(\psi)$ with respect to ξ, it is obtained that

$$f_\xi(\psi) = \frac{v_0 T(v_0^2 + T^2 - 2v_0 T\xi)^{\frac{1}{2}}(T^2 + v_0 T\xi - 2v_0^2)}{(v_0^2 - v_0 T\xi)^2}$$

Because $\xi \in [-1, 1]$, it can be observed that $f_\xi(\psi) < 0$. When $\xi = -1$, the function $f(\psi)$

reaches the maximum. Therefore, $f(\psi) \leq \frac{(v_0+T)^2}{v_0}$, which completes the proof of Lemma 1.

Lemma 1 will be used to provide a bound for the relative course rate while the heading rate input constraint is provided. Next, the performance of the UAV under the proposed controller will be explored.

Firstly, the condition that the UAV locates at the position $r = 0$ at $t = t_0$ needs to be discussed. According to the definition of the vector field, the relative course error $\chi_e = 0$ when $r = 0$. Moreover, it can be obtained that

$$\begin{aligned}\lim_{t\to t_0^+} \chi_d(t) &= \lim_{t\to t_0^+} \theta + \lim_{r\to 0} \phi = \lim_{t\to t_0^+} \arctan2(y_r, x_r)\\ &= \lim_{t\to t_0^+} \arctan2(\dot{y}_r, \dot{x}_r)\\ &= \chi(t_0) = \chi_d(t_0). \end{aligned} \tag{15}$$

and when $\chi_e = 0$, the desired relative course rate at $t \geq t_0$:

$$\dot{\chi}_d = \frac{4v_r r_d^3}{(r^2 + r_d^2)^2}. \tag{16}$$

Equation 15 implies that the desired relative course χ_d is right continuous at $r = 0$ with respect to t. Thus if the relative course rate is chosen as $\dot{\chi} = \dot{\chi}_d$, the UAV will always follow the vector field, i.e. $\chi = \chi_d$ for $t \geq t_0$. According to Lemma 1, the following can be derived

$$\begin{aligned} u_2 &= \frac{\dot{\chi}_d}{\lambda(\psi)} = \frac{4v_r r_d^3}{(r^2 + r_d^2)^2 \lambda(\psi)}\\ &\leq \frac{4(v_0 + T)^2}{v_0 r_d}. \end{aligned} \tag{17}$$

It can be observed from Eq. 17 that the proposed heading rate controller Eq. 13 provides the desired relative course rate. Therefore, if the UAV locates at the position $r = 0$ at t_0, the proposed heading rate controller will guarantee the UAV to follow the vector field for $t > t_0$, which in turn implies that the UAV will converge to the desired circular orbit.

Now, it is ready to consider the condition that the UAV locates at the position $r > 0$. Since $\dot{\chi}_d$ is the feedforward term of the heading rate controller, it is necessary to analyze its property. It is noted from Eq. 10 that, the desired relative course rate is related to the relative course error. The following lemma will study this relation and provide bounds for the desired relative course rate. □

Lemma 2 *For the system given by Eq. 4 and the vector field given by Eq. 6, there exists a positive constant $k_1 > 0$ such that,*

$$\dot{\chi}_d \leq \lambda(\psi) w_{\max} + k_1 \sin\chi_e, \quad \chi_e \in [-\pi, 0) \tag{18}$$

and

$$\dot{\chi}_d \geq -\lambda(\psi) w_{\max} + k_1 \sin\chi_e, \quad \chi_e \in [0, \pi) \tag{19}$$

Proof According to Lemma 1 and the maximum heading rate Eq. 12, the following inequality can be obtained.

$$\lambda(\psi) w_{\max} \geq \frac{4(v_0 + T)^2 \lambda(\psi)}{v_0 r_d} \geq \frac{4v_r}{r_d}$$

The proof will be discussed on two cases in terms of the relative course error.

Case 1 $\chi_e \in [0, \pi)$

When $\chi_e = 0$, $\dot{\chi}_d = \frac{4v_0 r_d^3}{(r^2+r_d^2)^2} \geq -\lambda(\psi) w_{\max} + k_1 \sin\chi_e$, which implies that k_1 can be any positive constant.

When $\chi_e \in (0, \pi)$, $f(\chi_e, r)$ is defined as follows:

$$\begin{aligned} &f(\chi_e, r)\\ &= \frac{1}{\sin\chi_e}\left(\dot{\chi}_d + \frac{4v_r}{r_d}\right)\\ &= \frac{1}{\sin\chi_e}\left\{\frac{v_r}{r}[\sin(\phi + \chi_e) + \sin\phi\cos(\phi + \chi_e)]\right.\\ &\qquad \left. + \frac{4v_r}{r_d}\right\}. \end{aligned}$$

If $f(\chi_e, r)$ has a positive lower bound, it implies that there exists a positive constant k_1 which makes the inequality 19 hold. Next, $f(\chi_e, r)$ is shown to have a positive lower bound. Partial differentiating the function $f(\chi_e, r)$ with respect to χ_e, it yields that

$$\frac{\partial f(\chi_e, r)}{\partial \chi_e} = \frac{-4v_r r_d^3}{(r^2 + r_d^2)^2 \sin^2\chi_e} + \frac{-4v_r \cot\chi_e}{r_d \sin\chi_e} \tag{20}$$

It is noted from Eq. 20 that, when $\cos\chi_e = \frac{-r_d^4}{(r^2+r_d^2)^2}$, $f(\chi_e, r)$ reaches its minimum value with respect to χ_e. Then the following inequality can be obtained.

$$\begin{aligned} & f(\chi_e, r) \\ & \geq f(\chi_e, r)|_{\cos\chi_e = \frac{-r_d^4}{(r^2+r_d^2)^2}} \\ & \geq \frac{v_r}{r}\left[\frac{r_d^4 - r^4 - 4r^2r_d^2}{(r^2+r_d^2)^2}\right] + \frac{4v_r}{r_d}\left[1 - \frac{r_d^8}{(r^2+r_d^2)^4}\right]^{\frac{1}{2}} \\ & \geq \frac{v_r}{r_d}\left[\frac{r_d^5 - r^4 r_d - 4r^2 r_d^3}{r(r^2+r_d^2)^2} + \frac{4(r^4 + 2r_d^2 r^2)}{(r^2+r_d^2)^2}\right] \\ & = \frac{v_r}{r_d}\left[1 + \frac{r_d^5 - r_d^4 r - 4r_d^3 r^2 + 6r_d^2 r^3 - r_d r^4 + 3r^5}{r(r^2+r_d^2)^2}\right] \end{aligned}$$

For the sake of simplicity, let $x = \frac{r}{r_d} > 0$, and it yields that

$$\begin{aligned} f(\chi_e, r) &\geq f(x) \\ &= \frac{v_r}{r_d}\left[1 + \frac{1 - x - 4x^2 + 6x^3 - x^4 + 3x^5}{x(x^2+1)^2}\right] \\ &> \frac{v_r}{r_d} > 0 \end{aligned}$$

Thus, there exists a positive constant $0 < k_1 \leq min\left\{\frac{v_r}{r_d}\right\}$ such that the inequality 19 holds.

Case 2 $\chi_e \in [-\pi, 0)$

The proof for this case is similar to the former case. In order to simplify the proof procedure, the following function is defined:

$$g(\chi_e) = \begin{cases} \dot{\chi}_d - \lambda(\psi)w_{\max} - k_1 \sin\chi_e, \chi_e \in [-\pi, 0) \\ \dot{\chi}_d + \lambda(\psi)w_{\max} - k_1 \sin\chi_e, \chi_e \in [0, \pi) \end{cases} \tag{21}$$

It is noted from Eq. 21 that $g(\chi_e) = -g(\chi_e + \pi)$ when $\chi_e \in [-\pi, 0)$. Moreover, according to the result of the case 1, it can be derived that

$$\begin{aligned} g(\chi_e) &= \dot{\chi}_d + \lambda(\psi)w_{\max} - k_1 \sin\chi_e \\ &\geq 0, \quad \chi_e \in [0, \pi). \end{aligned}$$

If $\chi_e \in [-\pi, 0)$, then $\chi_e + \pi \in [0, \pi)$. With the function 21, it yields that

$$\begin{aligned} g(\chi_e) &= \dot{\chi}_d - \lambda(\psi)w_{\max} - k_1 \sin\chi_e \\ &= -g(\chi_e + \pi) \leq 0, \end{aligned}$$

which implies that the inequality 18 holds. Thus the proof for this lemma is completed.

Lemma 2 analyzes the property of the desired relative course rate. Based on this analysis, the convergence of the relative course angle to the desired relative course under the proposed heading rate controller will be investigated in the sequel. □

Lemma 3 *If the control law (13) is applied to the system 4, there exists a positive constant $k_2 > 0$ with $k_2 \leq \frac{k}{2}$ and $k_2 \leq k_1$ such that $\dot{\chi}_e \geq -k_2 \sin\chi_e$, $\chi_e \in [-\pi, 0)$; $\dot{\chi}_e \leq -k_2 \sin\chi_e$, $\chi_e \in [0, \pi)$.*

Proof According to the definition of χ_e, the derivative of the relative course error can be obtained by

$$\dot{\chi}_e = \dot{\chi} - \dot{\chi}_d. \tag{22}$$

The heading rate controller Eq. 13 is transformed to the constrained relative course rate controller.

$$\begin{aligned} \dot{\chi} &= \lambda(\psi)\dot{\psi} \\ &= \begin{cases} \Omega & \text{if } |\Omega| \leq \lambda(\psi)w_{\max} \\ sgn(\Omega)\lambda(\psi)w_{\max} & \text{if } |\Omega| > \lambda(\psi)w_{\max} \end{cases} \end{aligned} \tag{23}$$

where $\Omega = -k\lambda(\psi)\chi_e + \dot{\chi}_d$. By combining the result of Lemma 2 and the constrained relative course rate controller Eq. 23, the proof of Lemma 3 is given as follows:

Case 1 $\chi_e \in [-\pi, 0)$

If $-k\lambda(\psi)\chi_e + \dot{\chi}_d > \lambda(\psi)w_{\max}$, $\dot{\chi}_e = \lambda(\psi)w_{\max} - \dot{\chi}_d \geq -k_1 \sin\chi_e \geq -k_2 \sin\chi_e$;

else if $-k\lambda(\psi)\chi_e + \dot{\chi}_d < -\lambda(\psi)w_{\max}$, $\dot{\chi}_e = -\lambda(\psi)w_{\max} - \dot{\chi}_d \geq -k\lambda(\psi)\chi_e \geq -k_2 \sin\chi_e$;

else $|-k\lambda(\psi)\chi_e + \dot{\chi}_d| \leq \lambda(\psi)w_{\max}$, $\dot{\chi}_e = -k\lambda(\psi)\chi_e \geq -k_2 \sin\chi_e$.

Case 2 $\chi_e \in [0, \pi)$

If $-k\lambda(\psi)\chi_e + \dot{\chi}_d > \lambda(\psi)w_{\max}$, $\dot{\chi}_e = \lambda(\psi)w_{\max} - \dot{\chi}_d < -k\lambda(\psi)\chi_e \le -k_2 \sin\chi_e$;
else if $-k\lambda(\psi)\chi_e + \dot{\chi}_d < -\lambda(\psi)w_{\max}$, $\dot{\chi}_e = -\lambda(\psi)w_{\max} - \dot{\chi}_d \le -k_1 \sin\chi_e \le -k_2 \sin\chi_e$;
else $|-k\lambda(\psi)\chi_e + \dot{\chi}_d| \le \lambda(\psi)w_{\max}$, $\dot{\chi}_e = -k\lambda(\psi)\chi_e \le -k_2 \sin\chi_e$. □

Remark Lemma 3 provides the slowest convergence rate bound for the relative course error. In practice, the convergence rate may be much faster than this given rate. For example, when $\chi_e = \pi$, it can be observed that $\dot{\chi}_d = \frac{4v_r r_d^3}{(r^2+r_d^2)^2}$ and $\dot{\chi}_e = \min\left\{k\lambda(\psi)\pi, \lambda(\psi)w_{\max} + \frac{4v_r r_d^3}{(r^2+r_d^2)^2}\right\} > 0$.

Lemma 3 shows that the relative course error will asymptotically converge to zero. However, the time when the relative course error converges to zero has not been determined. In addition, the problem that whether the distance between the UAV and the target will approach infinity while the relative course error converges to zero needs to be discussed. Therefore, the following lemma is introduced to determine the bound of the distance r.

Lemma 4 *Given an initial relative course error $\chi_{e0} \in (-\pi, \pi)$, if the control law 13 is applied to the system 4, the distance r in Eq. 5 has an upper bound $r_{\sup}$, where*

$$r_{\sup} = r_0 + \frac{v_0 + T}{k_2} \ln\left|\frac{\tan(\frac{\chi_{e0}}{2})}{\tan(\frac{\phi_0}{2} - \frac{\pi}{4})}\right|.$$

Proof It is noted from Lemma 3 that, for $\chi_{e0} \in (-\pi, \pi)$, the relative course error χ_e varies according to the following inequality:

$$\left|\tan\left(\frac{\chi_e}{2}\right)\right| \le \left|\tan\left(\frac{\chi_{e0}}{2}\right)\right| e^{-k_2 t}. \tag{24}$$

Case 1 $|\chi_{e0}| \in [0, \frac{\pi}{2}]$

It is assumed that the initial distance $r_0 > r_d$. If $r > r_d$ and $\chi_{e0} \in [0, \frac{\pi}{2}]$, $\cos(\phi + \chi_e) < 0$. Then it is observed from Eq. 5 that $r < r_0$. If $\chi_{e0} \in [-\frac{\pi}{2}, 0]$, it can be derived from Eq. 24 that r has an upper bound as follows:

$$r \le (v_0 + T)t_1 + r_0. \tag{25}$$

where $t_1 = \frac{1}{k_2} \ln\left|\frac{\tan(\frac{\chi_{e0}}{2})}{\tan(\frac{\phi_0}{2} - \frac{\pi}{4})}\right|$ and $\phi_0 = \arctan(\frac{r_0}{r_d})$.

Case 2 $|\chi_{e0}| \in (\frac{\pi}{2}, \pi)$

For this case, the time t_2 when the relative course error $|\chi_{e0}|$ decreases to $\frac{\pi}{2}$ is analyzed. It can be obtained from Eq. 24 that

$$t_2 = \frac{1}{k_2} \ln\left|\tan(\frac{\chi_{e0}}{2})\right|. \tag{26}$$

Combining these two cases, the upper bound of the distance r can be computed via the following calculation.

$$\begin{aligned} r &\le r_{sup} = r_0 + (v_0 + T)(t_1 + t_2) \\ &= r_0 + \frac{v_0 + T}{k_2} \ln\left|\frac{\tan(\frac{\chi_{e0}}{2})}{\tan(\frac{\phi_0}{2} - \frac{\pi}{4})}\right|. \end{aligned} \tag{27}$$

In this lemma, the condition that $\chi_e = -\pi$ is not considered. In fact, when $\chi_e = -\pi$, $\dot{\chi}_e > 0$, which implies that after a short time t_3, the relative course error $\chi_e \in (-\pi, \pi)$. It also implies that $r \le r_{sup} + (v_0 + T)t_3$ when the initial relative course error $\chi_{e0} = -\pi$.

Now, it is ready to prove the stability of the proposed vector field approach with control input constraints in the presence of moving target velocity. □

Theorem 5 *Given an initial relative course error $\chi_{e0} \in (-\pi, \pi)$, the system given by Eqs. 4 and 2 with u_2 given by Eq. 13 and χ_d given by Eq. 6 asymptotically converges to the desired trajectory, i.e. $r \to r_d$ and $\chi \to \chi_d$.*

Proof Consider the Lyapunov function candidate:

$$V = \frac{1}{2}(r - r_d)^2 + \frac{\mu}{2}\chi_e^2. \tag{28}$$

The proof will be provided on two cases in terms of the relative course error χ_e.

Case 1 $|\chi_e| \in (\frac{\pi}{2}, \pi)$

Differentiating the function V with respect to time, it yields that

$$\begin{aligned}\dot{V} &= (r-r_d)\dot{r} + \mu\chi_e\dot{\chi}_e \\ &\le (r-r_d)v_r\cos(\phi+\chi_e) - \mu k_2\chi_e\sin\chi_e \\ &< (r_{sup}+r_d)(v_0+T) - \mu k_2\frac{\pi}{2}\sin\chi_{e0}.\end{aligned}$$

Let $\mu \ge \frac{2(r_{sup}+r_d)(v_0+T)}{k_2\pi\sin\chi_{e0}}$, then $\dot{V} < 0$.

Case 2 $|\chi_e| \in [0, \frac{\pi}{2}]$

$$\begin{aligned}\dot{V} &= (r-r_d)\dot{r} + \mu\chi_e\dot{\chi}_e \\ &\le -\mu k_2\chi_e\sin\chi_e - \frac{(r-r_d)^2(r+r_d)v_r\cos(\chi_e)}{r^2+r_d^2} \\ &\quad - \frac{2(r-r_d)rr_dv_r\sin(\chi_e)}{r^2+r_d^2} \\ &\le -\mu k_2\chi_e\sin\chi_e - \frac{(r-r_d)^2(r+r_d)v_r}{r^2+r_d^2} \\ &\quad - 2v_r(r-r_d)\sin\frac{\chi_e}{2}\sin\left(\frac{\chi_e}{2}+\phi\right) \\ &\le -\frac{(r-r_d)^2(r+r_d)v_r}{r^2+r_d^2} + 2v_r|r-r_d|\left|\sin\frac{\chi_e}{2}\right| \\ &\quad - 2\mu k_2\sin^2\left(\frac{\chi_e}{2}\right)\end{aligned}$$

Let $\mu \ge \frac{(r_{sup}^2+r_d^2)(v_0+T)}{k_2(r_{sup}+r_d)}$, then

$$\begin{aligned}\dot{V} &\le -\mu k_2\sin^2\left(\frac{\chi_e}{2}\right) \\ &\quad - \left\{\left[\frac{(r+r_d)v_r}{r^2+r_d^2}\right]^{\frac{1}{2}}|r-r_d| \right. \\ &\qquad \left. - \left[\frac{(r^2+r_d^2)v_r}{r+r_d}\right]^{\frac{1}{2}}\left|\sin\left(\frac{\chi_e}{2}\right)\right|\right\}^2 \\ &\le 0. \end{aligned} \tag{29}$$

It can be observed from the cases 1 and 2 that, when $\mu \ge max\left\{\frac{2(r_{\sup}+r_d)(v_0+T)}{k_2\pi\sin\chi_{e0}}, \frac{(r_{\sup}^2+r_d^2)(v_0+T)}{k_2(r_{\sup}+r_d)}\right\}$, the corresponding time derivative of the Lyapunov function V is always nonpositive, i.e. $\dot{V} \le 0$. It is also noted from Eq. 29 that, $\dot{V} = 0$ implies that $r = r_d$ and $\chi_e = 0$. By LaSalle's Invariance principle, it can be obtained that $r \to r_d$ and $\chi \to \chi_d$ asymptotically. □

Remark Theorem 5 does not consider the condition that $\chi_e{=}{-}\pi$. However, when $\chi_e{=}{-}\pi$, $\dot{\chi}_e{>}$ 0, which implies that $\chi_e = -\pi$ is not an equilibrium point and can asymptotically converge to 0. Moreover, the condition that $r = 0$ also has been discussed in this section. Therefore, the proposed heading rate controller can guarantee the global convergence of the UAV to the desired circular orbit.

4 Adaptive Estimate for Moving Target Velocity

In the previous section, the ground target tracking in the presence of known constant moving target velocity is discussed. In this section, an adaptive observer will be developed to estimate unknown moving target velocity. Generally, the UAV airspeed is faster than the moving target velocity and the proposed control approach also requires that the moving target velocity is slower than the nominal airspeed v_0. Therefore, during the estimation, the estimate of the moving target velocity should be bounded.

The UAV kinematic model 3 is used in this section with an unknown moving target velocity (T_x, T_y). Here, T_x and T_y are constant and it is assumed that there exists an upper bound T^* such that $|T_x| \le T^*$ and $|T_y| \le T^*$. $(\widehat{T}_x, \widehat{T}_y)$ is introduced to denote the estimate of (T_x, T_y), and then the actual moving target velocity and its estimate are defined as follows [20]:

$$T_x = T^*\tanh\varphi_x,\ T_y = T^*\tanh\varphi_y \tag{30}$$

$$\widehat{T}_x = T^*\tanh\widehat{\varphi}_x,\ \widehat{T}_y = T^*\tanh\widehat{\varphi}_y \tag{31}$$

where φ_x and φ_y are unknown constants, as well as $\widehat{\varphi}_x$ and $\widehat{\varphi}_y$ are the corresponding estimates. Here, hyperbolic function $\tanh(x)$ is introduced to bound the estimates.

The adaptive observer can be formulated by the following equations:

$$\begin{cases}\dot{\widehat{x}}_r = u_1\cos\psi - \widehat{T}_x + k_3\widetilde{x}_r \\ \dot{\widehat{y}}_r = u_1\sin\psi - \widehat{T}_y + k_4\widetilde{y}_r\end{cases} \tag{32}$$

where $\widetilde{x}_r = x_r - \widehat{x}_r$ and $\widetilde{y}_r = y_r - \widehat{y}_r$.

By combining the UAV model 3 and the proposed adaptive observer Eq. 32 with the adaptive

update laws $\dot{\widehat{\varphi}}_x$ and $\dot{\widehat{\varphi}}_y$, the corresponding error dynamics is derived as follows:

$$\begin{aligned} \dot{\tilde{x}}_r &= -\dot{\widetilde{T}}_x - k_3\dot{\tilde{x}}_r, \quad & \dot{\tilde{y}}_r &= -\dot{\widetilde{T}}_y - k_4\dot{\tilde{y}}_r; \\ \dot{\widehat{\varphi}}_x &= -\gamma\dot{\tilde{x}}_r, & \dot{\widehat{\varphi}}_y &= -\gamma\dot{\tilde{y}}_r. \end{aligned} \tag{33}$$

where $\widetilde{T}_x = T_x - \widehat{T}_x$ and $\widetilde{T}_y = T_y - \widehat{T}_y$. Now, it is ready to verify the stability of the adaptive observer. Consider the following function

$$\begin{aligned} V = {} & \frac{1}{2}\tilde{x}_r^2 + \frac{1}{2}\tilde{y}_r^2 + \frac{1}{\gamma}T^*(\log\cosh\widehat{\varphi}_x - \widehat{\varphi}_x\tanh\varphi_x) \\ & + \frac{1}{\gamma}T^*(\log\cosh\widehat{\varphi}_y - \widehat{\varphi}_y\tanh\varphi_y). \end{aligned} \tag{34}$$

By differentiating this function V with respect to time t, it is obtained that

$$\begin{aligned} \dot{V} &= \tilde{x}_r\dot{\tilde{x}}_r + \tilde{y}_r\dot{\tilde{y}}_r + \frac{1}{\gamma}T^*(\dot{\widehat{\varphi}}_x\tanh\widehat{\varphi}_x - \dot{\widehat{\varphi}}_x\tanh\varphi_x) \\ &\quad + \frac{1}{\gamma}T^*(\dot{\widehat{\varphi}}_y\tanh\widehat{\varphi}_y - \dot{\widehat{\varphi}}_y\tanh\varphi_y) \\ &= \tilde{x}_r(-\dot{\widetilde{T}}_x - k_3\dot{\tilde{x}}_r) + \tilde{y}_r(-\dot{\widetilde{T}}_y - k_4\dot{\tilde{y}}_r) \\ &\quad - \frac{1}{\gamma}\widetilde{T}_x\dot{\widehat{\varphi}}_x - \frac{1}{\gamma}\widetilde{T}_y\dot{\widehat{\varphi}}_y \\ &= -k_3\tilde{x}_r^2 - k_4\tilde{y}_r^2 \le 0. \end{aligned}$$

Next, it will be shown that the function V is lower bounded. Firstly, the following function $f(x) = \log\cosh x - x\tanh x_0$ is defined. Differentiating the function $f(x)$ with respect to x, it yields that

$$f_x(x) = \frac{df(x)}{dx} = \tanh x - \tanh x_0. \tag{35}$$

It is observed from Eq. 35 that, when $x = x_0$, $f(x)$ reaches the minimum. Thus, the third and the fourth terms in the function 34 have minimum values when $\widehat{\varphi}_x = \varphi_x$ and $\widehat{\varphi}_y = \varphi_y$. Hence,

$$\begin{aligned} V &\ge \frac{T^*}{\gamma}\big(\log\cosh\varphi_x - \varphi_x\tanh\varphi_x \\ &\qquad + \log\cosh\varphi_y - \varphi_y\tanh\varphi_y\big) \\ &\ge \frac{-2T^*}{\gamma}\log 2. \end{aligned} \tag{36}$$

Therefore, the function V is lower bounded. Moreover, $\ddot{V} = 2k_3\tilde{x}_r(\widetilde{T}_x + k_3\tilde{x}_r) + 2k_4\tilde{y}_r(\widetilde{T}_y + k_4\tilde{y}_r)$ is bounded. Thus, by Barbalat's lemma [19], it can be shown that $\dot{V} \to 0$ as $t \to \infty$, which also implies that $\tilde{x}_r \to 0$ and $\tilde{y}_r \to 0$.

In addition, $\ddot{\tilde{x}}_r = -\ddot{\widetilde{T}}_x - k_3\ddot{\tilde{x}}_r = k_3(\dot{\widetilde{T}}_x + k_3\dot{\tilde{x}}_r) - \frac{4T^*\gamma\tilde{x}_r}{(e^{\widehat{\varphi}_x} + e^{-\widehat{\varphi}_x})^2}$, which implies that $\ddot{\tilde{x}}_r$ is bounded. By Barbalat's lemma, it can be obtained that, $\dot{\tilde{x}}_r = -\dot{\widetilde{T}}_x - k_3\dot{\tilde{x}}_r \to 0$, which in turn implies that $\dot{\widetilde{T}}_x \to 0$. Similarly, it can also be shown that $\dot{\widetilde{T}}_y \to 0$.

Based on this proposed adaptive observer, the corresponding controller for ground target tracking is designed as Eq. 13. The overall control architecture is illustrated in Fig. 2.

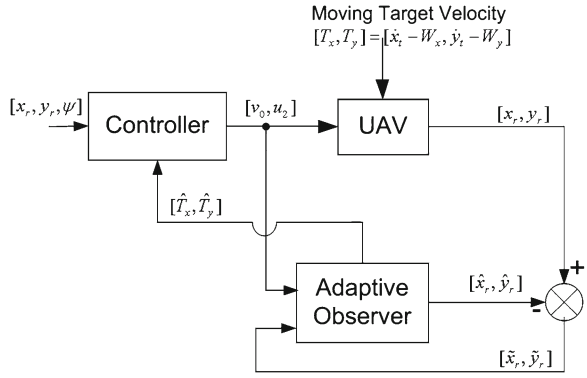

Fig. 2 Target tracking control architecture based on an adaptive observer

5 Simulation Results

In this section, simulation results are presented to demonstrate the effectiveness of the proposed approach. The simulation includes four scenarios: scenario one describes ground target tracking with known constant moving target velocity; both of scenario two and scenario three describe ground target tracking where the measurement noise of the relative position and the uncertainty of the moving target velocity are taken into account. It is assumed that the nominal moving target velocity is known in scenario two while it is unknown in scenario three. In scenario four, the moving target velocity is not constant and varies with time. Table 1 shows the specifications of the UAV and control law parameters.

Table 1 Specifications of the UAV and control law parameters

Parameter	Value
Nominal airspeed v_0	20 m/s
Maximum heading rate $w_{\max}$	0.5 rad/s
Desired distance r_d	400 m
Heading rate feedback gain k	0.2
Target velocity	(2, 3) m/s
Background wind	$(-5, -2)$ m/s
Upper bound T^*	10 m/s

5.1 Scenario One

In this scenario, the UAV starts the mission of ground target tracking at the relative position $(x_r, y_r) = (10, 0)$m with initial heading angle $\psi_0 = \frac{\pi}{2}$. Figure 3 shows the trajectory of the UAV with respect to the moving target in the presence of background wind. It can be observed from Fig. 3 that the UAV finally converges to the desired circular orbit. Correspondingly, Fig. 4 shows the trajectory of the UAV with respect to the inertial coordinate frame. As illustrated in Fig. 5, the heading rate controller reaches saturation at the beginning of the tracking mission and finally heading rate converges to the desired heading rate. In addition, as depicted in Fig. 6 that the relative course error asymptotically converges to zero even in the presence of large initial relative course error. It is worth noting that, a sinusoidal function is used to bound the convergence rate in the Section 3, but usually the actual convergence rate is much faster than this bound.

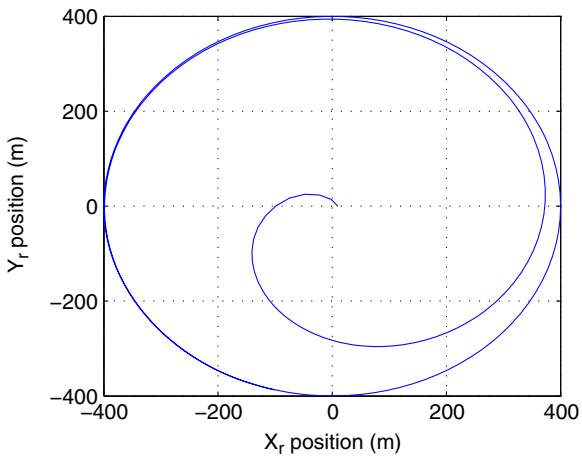

Fig. 3 Trajectory w.r.t target

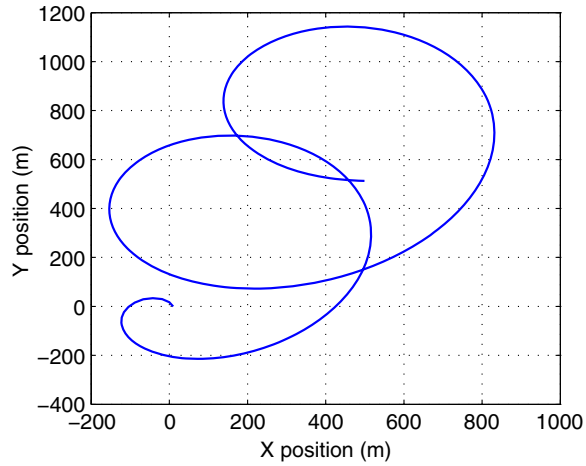

Fig. 4 Trajectory w.r.t inertial frame

5.2 Scenario Two

In scenario one, the relative position of the UAV with respect to the target and the moving target velocity are assumed to be known accurately. However, the measurement noise and the uncertainty of the wind always exist in practice. Therefore, the measurement noise of the relative position (x_r, y_r) and the uncertainty of the moving target velocity (T_x, T_y) have to be considered. In this scenario, bounded random uncertainties $\delta T_x, \delta T_y \in (-2, 2)$m/s are added to the moving target velocity and zero mean random measurement errors with a variance $\Delta = 4$ are introduced as the noise in the relative position measurement.

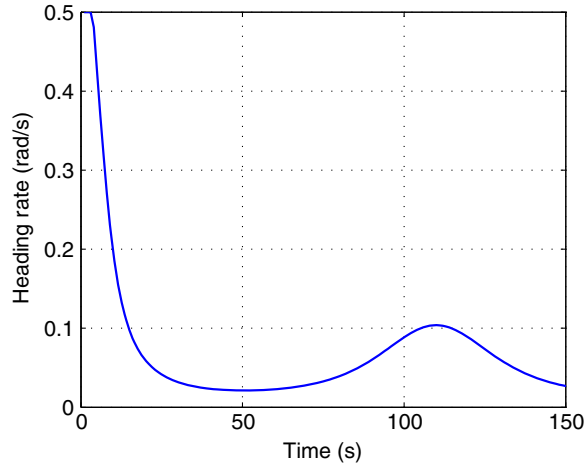

Fig. 5 Heading rate control input

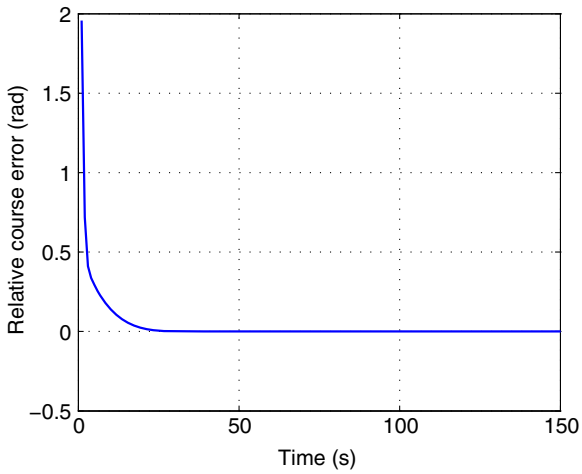

Fig. 6 Relative course error

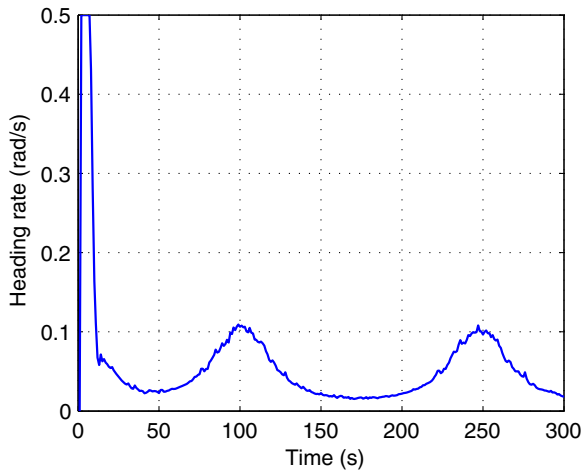

Fig. 8 Heading rate

Moreover, it is well known that the heading rate of the UAV is dependant on the roll angle. Thus, in this scenario, $\ddot{\psi} = k_5(\dot{\psi}_c - \dot{\psi})$ will be used to approximate the dynamics of the heading rate, where $\dot{\psi}_c$ is the commanded heading rate Eq. 13 and $k_5 = 1$. Figure 7 shows that the distance between the UAV and the target converges to the neighborhood of the desired distance r_d. As depicted in Fig. 8, the heading rate still reaches saturation at the beginning of the mission. When the control gain k_5 is small enough, the heading rate will not reach saturation. However, it will take much longer time for the UAV to converge to the desired orbit.

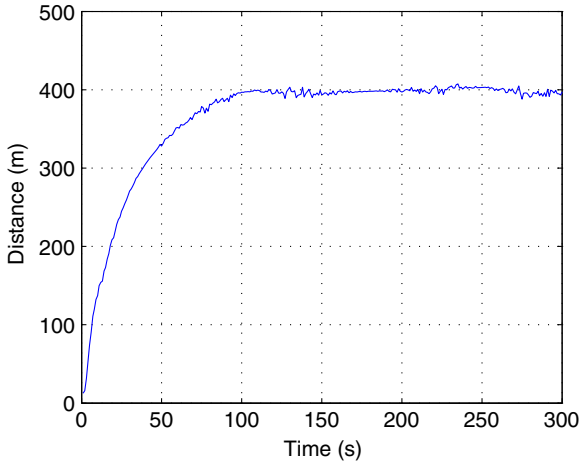

Fig. 7 Actual distance

5.3 Scenario Three

In this scenario, the nominal moving target velocity is unknown. Thus, an adaptive observer is designed to estimate the unknown moving target velocity. The actual moving target velocity is $(7 + \delta T_x, 5 + \delta T_y)$m/s and the relative position measurement noise is the same as that in scenario two. It can be observed from Fig. 9 that although the moving target velocity is unknown and is not constant, the UAV still can converge to the neighborhood of the desired orbit. Figure 10 shows that, the adaptive estimate for the moving target velocity does not converge to the nominal velocity as the moving target velocity is not constant.

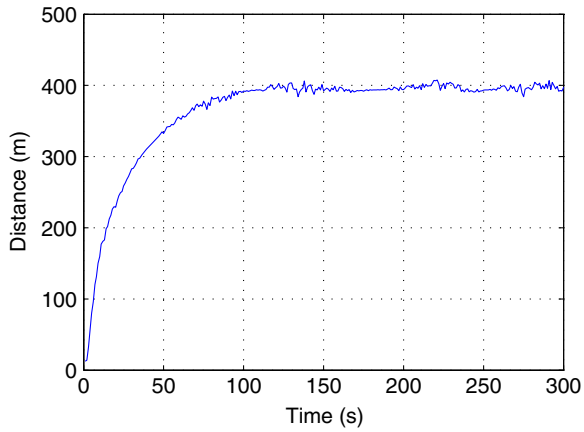

Fig. 9 Actual distance

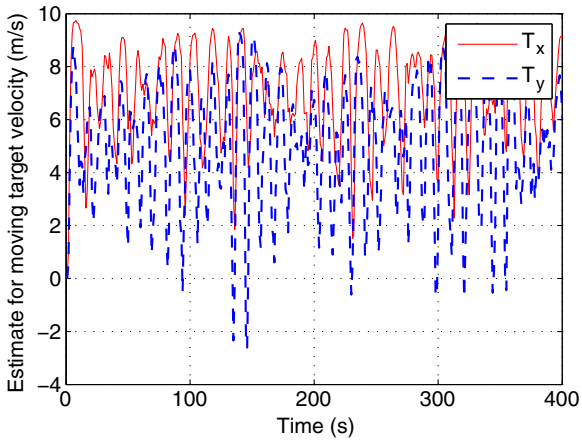

Fig. 10 Adaptive estimate

However, the adaptive estimate varies around the nominal velocity (7, 5)m/s.

5.4 Scenario Four

In this scenario, the moving target velocity is unknown and varies with time. Thus, the adaptive observer is still used to estimate the unknown moving target velocity. The actual moving target velocity is $(7\cos(\pi t/150), 5\cos(\pi t/250))$m/s. Figure 11 shows that the distance between UAV and target oscillates in the vicinity of the desired distance due to the time varying moving target velocity. However, the proposed adaptive observer can accurately estimate this moving target velocity as shown in Fig. 12.

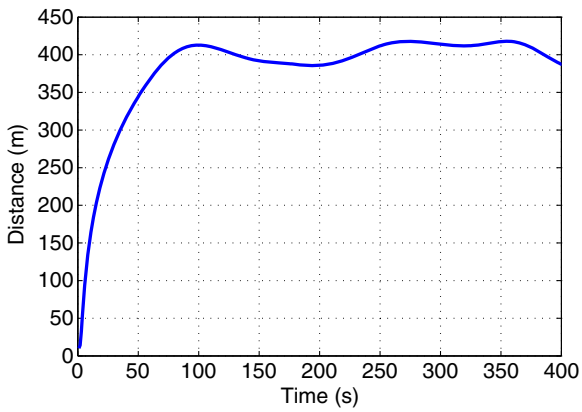

Fig. 11 Distance

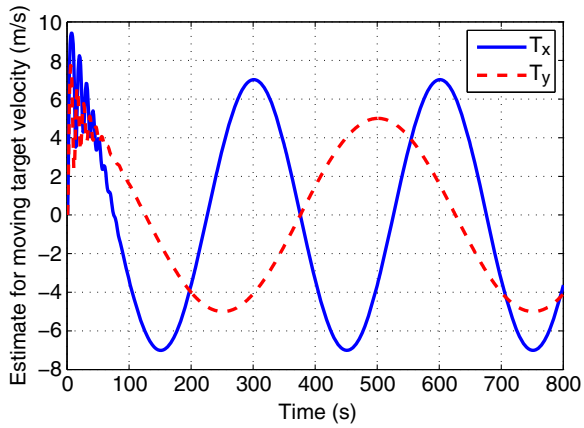

Fig. 12 Adaptive estimate

6 Conclusions

This paper shows that a saturated heading rate controller based on guidance vector field is able to achieve stable ground target tracking in the presence of background wind. The global asymptotical convergence of the system with any initial position and heading angle is guaranteed by the proposed saturated heading rate controller. In addition, a constrained adaptive observer is constructed to estimate unknown moving target velocity. The constrained adaptive estimate makes the proposed saturated heading rate controller feasible. Simulation results show that the proposed approach is robust to the uncertainty of the system and suitable for the dynamic model.

References

1. Beard, R.W., McLain, T.W., Goodrich, M., Anderson, E.P.: Coordinated target assignment and intercept for unmanned air vehicles. IEEE Trans. Robot. Autom. **18**(6), 911–922 (2002)
2. Beard, R.W., McLain, T.W., Nelson, D.B., Kingston, D., Johanson, D.: Decentralized cooperative aerial surveillance using fixed-wing miniature UAVs. Proc. IEEE **94**(7), 1306–1324 (2006)
3. Carole, G.P., Olivier, T., Andre, D., Eric, P.: Receding horizon model-based predictive control for dynamic target tracking: a comparative study. In: AIAA Guidance, Navigation, and Control Conference and Exhibit, Chicago (2009)

4. Doherty, P., Rudol, P.: A UAV search and rescue scenario with human body detection and geolocalization. In: Proc. 20th Australian Joint Conference on AI (2007)
5. Frew, E., Lawrence, D.: Cooperative standoff tracking of moving targets using Lyapunov guidance vector fields. AIAA J. Guid. Control Dyn. **31**(2), 290–306 (2008)
6. Girard, A.R., Howell, A.S., Hedrick, J.K.: Border patrol and surveillance missions using multiple unmanned air vehicles. In: Proceedings of the 43rd IEEE Conference on Decision and Control, vol. 1, pp. 620–625 (2004)
7. Grocholsky, B., Keller, J., Kumar, V., Pappas, G.: Cooperative air and ground surveillance. IEEE Robot. Autom. Mag. **13**(3), 16–25 (2006)
8. Kingston, D., Beard, R.: UAV splay state configuration for moving targets in wind. In: Advances in Cooperative Control and Optimization, pp. 109–128 (2006)
9. Lawrence, D., Frew, E., Pisano, W.: Lyapunov vector fields for autonomous unmanned aircraft flight control. AIAA J. Guid. Control Dyn. **31**(5), 1220–1129 (2008)
10. Lee, S.O., Cho, Y.J., Hwang, B.M., You, B.J., Oh, S.R.: A stable target-tracking control for unicycle mobile robots. In: Proceedings of IEEE/RSJ International Conference on Intelligent Robots and Systems, pp. 1822–1827 (2000)
11. Nelson, D.R., Barber, D.B., McLain, T.W., Beard, R.W.: Vector field path following for miniature air vehicles. IEEE Trans. Robot. **23**(3), 519–529 (2007)
12. Park, S., Deyst, J., How, J.P.: A new nonlinear guidance logic for trajectory tracking. In: AIAA Guidance, Navigation, and Control Conference, vol. 2, pp. 941–956. Reston (2004)
13. Park, S., Deyst, J., How, J.P.: Performance and Lyapunov stability of a nonlinear path-following guidance method. AIAA J. Guid. Control Dyn. **30**(6), 1718–1728 (2007)
14. Proud, A.W., Pachter, M., D'Azzo, J.J.: Close formation flight control. In: Proc. AIAA Guidance, Navigation, and Control Conference, Portland (1999)
15. Rafi, F., Khan, S., Shafiq, K., Shah, M.: Autonomous target following by unmanned aerial vehicles. In: Proceedings of SPIE, vol. 6230, pp. 1–8. Orlando, Florida (2006)
16. Ren, W.: Trajectory tracking control for a miniature fixed-wing unmanned air vehicle. Int. J. Syst. Sci. **38**(4), 361–368(2007)
17. Ren, W., Beard, R.W.: Trajectory tracking for unmanned air vehicles with velocity and heading rate constraints. IEEE Trans. Control Syst. Technol. **12**(5), 706–716 (2004)
18. Rysdyk, R.: Unmanned aerial vehicle path following for target observation in wind. AIAA J. Guid. Control Dyn. **29**(5), 1092–1100 (2006)
19. Slotine, J.J.E., Li, W.: Applied Nonlinear Control. Prentice Hall, Englewood Cliffs (1991)
20. Summers, T.H., Akella, M.R., Mears, M.J.: Coordinated standoff tracking of moving targets: control laws and information architectures. AIAA J. Guid. Control Dyn. **32**(1), 56–69 (2009)
21. Zhu, S., Wang, D., Chen, Q.: Standoff tracking control of moving target in unknown wind. In: IEEE Conference on Decision and Control. Shanghai, China (2009)